Babinet-Inverted Optical Nanoantenna Analogue of Electromagnetically Induced Transparency *

Yin-Xing Ding(丁银兴)[1,2], Lu-Lu Wang(王鲁橹)[1,2], Li Yu(于丽)[1,2]**

[1]State Key Laboratory of Information Photonics and Optical Communications, Beijing University of Posts and Telecommunications, Beijing 100876

[2]School of Science, Beijing University of Posts and Telecommunications, Beijing 100876

(Received 1 September 2017)

A Babinet-inverted optical nanoantenna analogue of electromagnetically induced transparency based on the coupling between two magnetic dipole antennas and a magnetic octupole antenna in a Au film waveguide is demonstrated. Simulation results indicate that a pronounced elimination occurs in the radiating spectrum due to the coupling-induced radiation suppression. A two-oscillator electromagnetically induced transparency model is used to describe the antenna. The coupling coefficient between the magnetic dipole antennas and the magnetic octupole antenna is calculated using the model and is found to decline exponentially with the increase of the distance between them. Such an antenna can be directly integrated with optical waveguides or transmission lines, thus is of fundamental significance for the applications in nano-optics, such as the optical device miniaturizations and photonic circuit integrations.

PACS: 42.50.Gy, 42.82.Gw, 42.82.−m DOI: 10.1088/0256-307X/35/1/014201

The elimination of absorption via quantum interference in an atomic medium is known as electromagnetically induced transparency (EIT).[1−3] This phenomenon allows for a very narrow transparency resonance in the absorption spectrum, which is highly desirable for sensing applications.[4] In recent years, classical analogues of EIT have been realized through coupling-induced destruction interference between two resonances, such as a dipole antenna with a quadrupole[5−10] or octupole antenna.[11] In these classical analogues no pumping laser is necessary, which significantly decreases the complexity of experimental setups. However, most of the cases are based on periodic structures to provide an interference effect, which enlarges the volume and makes them hard to fabricate and be integrated with surface plasmons' (SPs) waveguides.

An optical antenna, a miniaturized analogy of a radio-frequency (RF) antenna working in the optical regime, provides a new method of manipulating visible and infrared radiation at the nanoscale due to the strong confinement of electromagnetic field.[12−18] Furthermore, its strong interaction with nano-emitters enables it to have great potential applications in nano-optics, such as focusing optical fields to subdiffraction-limited volumes,[19] enhancing the excitation and emission of quantum emitters,[20−23] directing their radiation,[24,25] and modifying their spectra.[26] Among the various optical antennas, the aperture-type optical antennas,[27,28] which can be considered as a Babinet-complementary counterpart of the rod-type optical antennas, have attracted various investigations, such as the Babinet-inverted optical Yagi-Uda antennas,[29] the directional Babinet-inverted optical nanoantennas integrated with plasmonic waveguides,[30] and the broadband directional SPs couplers.[27] Compared with the rod-type optical antennas, the aperture-type optical antennas can be directly fabricated on optical waveguides, thus are easy to fabricate and be integrated with optical waveguides.

In this work, we demonstrate that a Babinet-inverted optical nanoantenna analogue of EIT is achieved based on aperture-type antennas that are fabricated in an optical waveguide. The structure of the antenna consists of two vertical slots and a horizontal slot pair that are fabricated in a homogeneous Au film, as shown in Fig. 1. In accordance to Babinet's principle, the vertical slots serve as two magnetic dipole antennas since each of them supports a spectrally broad bright mode.[6,29] The horizontal slot pair supports a spectrally narrow dark mode and serves as a magnetic octupole antenna. The Au film serves as an optical waveguide, with which the SPs can be transmitted to the slots and excite the resonant modes of the vertical slots.[27,30] Due to close proximity, the magnetic dipole antennas and the magnetic octupole antenna are strongly coupled. As a result, destructive interference between two excitation pathways, namely, the direct excitation of the magnetic dipole antennas by the incident SPs and the excitation by coupling with the magnetic octupole antenna is induced, which leads to an elimination of the radiation. In fact, accurate terminology would suggest using the expression 'electromagnetically induced radiating elimination (EIRE) effects' for this phenomenon, as we in-

*Supported by the National Key Research and Development Program of China under Grant No 2016YFA0301300, the National Natural Science Foundation of China under Grant Nos 11374041, 11574035 and 11404030, and the State Key Laboratory of Information Photonics and Optical Communications.

**Corresponding author. Email: yuliyuli@bupt.edu.cn

© 2018 Chinese Physical Society and IOP Publishing Ltd

troduce induced radiation spectrum. Different from the previous related works, here the input of the configuration is traveling waves, and the output is free space light, thus it can be directly integrated with optical waveguides. This novel structure can enhance the coupling strength between the two kinds of antennas compared with Ref. [6], so it can work individually without using periodic structures to provide an interference effect, which is of great importance for optical device miniaturizations and photonic circuit integrations.

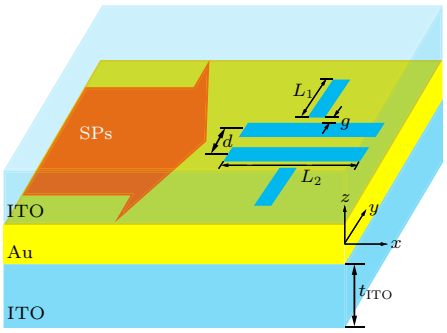

Fig. 1. Illustration of the Babinet-inverted optical nanoantenna configuration.

The geometry of the Babinet-inverted optical nanoantenna is illustrated in Fig. 1. It consists of two vertical slots and a horizontal slot pair in a 200-nm-thick Au film. Their lengths are $L_1 = 220\,\text{nm}$ and $L_2 = 460\,\text{nm}$, respectively, and their widths are 60 nm. The vertical slots are positioned in the middle of the horizontal slots, and the gaps between them are $g = 30\,\text{nm}$. The distance between the two horizontal slots is $d = 120\,\text{nm}$. The Au film is sandwiched by two indium-tin oxide (ITO) layers with the same thickness t_{ITO}=2 μm, and the slots are filled by ITO as well. The reason to choose ITO as the medium filling the slots is to facilitate this structure to be applied in sensors or non-linear optics due to its high nonlinear coefficient, while in the simulation the ITO is simply regarded as dielectric with a refractive index $n_{\text{ITO}} = 1.96$ in the infrared spectral regime.[27] A rectangular coordinate system xyz is defined based on the Au film, in which the midplane of the Au film is defined as xy-plane and the axis vertical to the Au film is defined as z-axis.

Resonant modes are supported by the cut-off structures. Their properties are simulated using the finite-difference time-domain (FDTD) method. The calculation results indicate that both of the vertical slots support the $m = 1$ modes, as shown in Fig. 2(a). Here m denotes the number of the antinodes along the long axis direction. Thus the vertical slots supporting resonant modes can be regarded as two magnetic dipole antennas, which are strongly coupled to light.[6,28,29] For the horizontal slot pair, a mode whose current distribution is anti-symmetrical with respect to y-axis and symmetrical with respect to x-axis is supported, as shown in Fig. 2(b). This mode originates from the coupling of the anti-symmetrical $m = 2$ mode supported by each of the horizontal slots. Thus the horizontal slot pair can be regarded as a magnetic octupole antenna, which is nonradiative in nature due to its anti-symmetry. The distributions of the x-component of electric field with respect to frequency obtained from the point illustrated by the white × in Fig. 2(a) and the y-component of electric field obtained from the points illustrated by the white • in Fig. 2(b) are shown in Figs. 2(c) and 2(d), respectively, which indicate that the resonance frequencies of the two modes are about 201 and 210 THz, respectively.

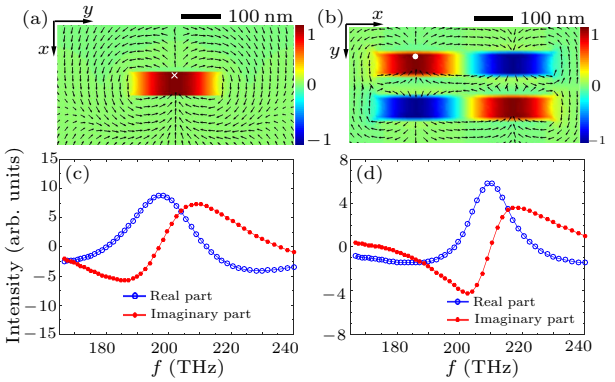

Fig. 2. Distributions of the (a) x-component and (b) y-component of electric field of the resonant mode supported by one of the vertical slots and the horizontal slot pair. The black arrows denote the instant direction of the current in the Au film. (c) Real part (blue curve) and imaginary part (red curve) of the x-component of the electric field obtained from the point illustrated by the white × in Fig. 2(a) versus frequency. (d) Real part (blue curve) and the imaginary part (red curve) of the y-component of the electric field obtained from the point illustrated by the white • in Fig. 2(b) versus frequency.

Energy of the incident SPs can be coupled to resonant modes and radiates out as light through the vertical slots.[27,30] Figure 3(a) illustrates the normalized radiation spectrum of the vertical slots that are isolated from the horizontal slot pair, in which a single resonance ($f_0 = 201\,\text{THz}$) is observable owing to the excitation of the $m = 1$ modes inside the vertical slots. By introducing the horizontal slot pair, the mode supported by it strongly couples with the modes supported by the vertical slots. As a result, destructive interference between the two excitation pathways, i.e., the direct excitation by the incident SPs and the excitation by coupling with the magnetic octupole antenna, leads to a radiating suppression of the vertical slots. Figures 3(b)–3(d) illustrate the normalized radiation spectra of the antenna when the horizontal slot pair is introduced, the corresponding distance g is 80, 50 and 20 nm, respectively. It is seen that a dip around $f_{\text{dip}} = 202\,\text{THz}$ emerges near the center of the broad resonance and becomes deeper as g reduced. It is worth mentioning that the frequency of the dip is slightly smaller than the isolated horizontal slot pair because the presence of the vertical slots affects the resonance condition of the horizontal slot pair.

To obtain further knowledge of the EIRE effect, the electric field amplitude distributions at the three frequencies (illustrated by A, B and C in Fig. 3(d)) are calculated and shown in Figs. 4(a)–4(c), respectively. It is seen that at the frequencies A ($f = 178$ THz) and C ($f = 217$ THz), the electric field in the vertical slots is stronger than the horizontal slot pair since they are excited by the incident SPs. At the frequency of B ($f = 202$ THz), the resonant mode of the horizontal slot pair is excited by coupling with the vertical slots, thus the electric field in the horizontal slot pair is significantly larger than the vertical slots. However, compared with the cases A and C, the electric field intensity inside the vertical slots is obviously suppressed due to the coupling-induced destructive interference with the horizontal slot pair.

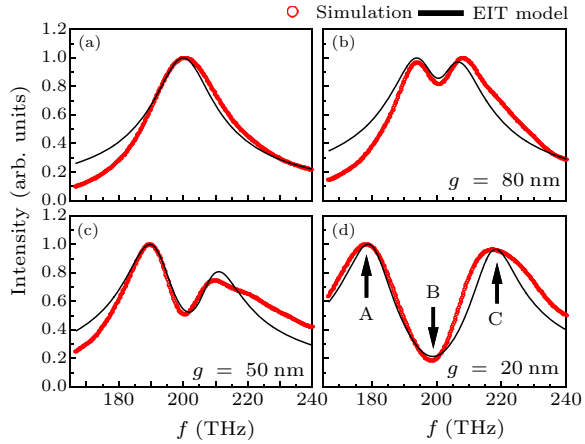

Fig. 3. (a) Radiation spectra of the nanoantenna without the horizontal slot pair. (b)–(d) Radiation spectra of the EIRE nanoantennas for different values of g. The red circles denote the simulation results and the black curves represent the results obtained by a two-oscillator EIT model.

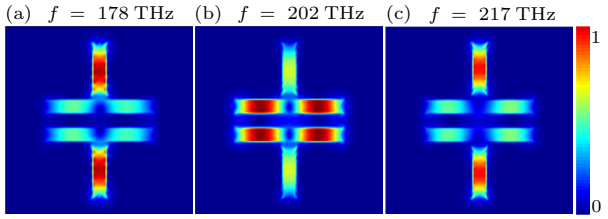

Fig. 4. (a)–(c) Electric field amplitude distributions in the slots when the antenna is excited by the incident SPs of the frequencies $f = 178$ THz, 202 THz and 217 THz, respectively. All of them are normalized by the same scale bar.

The geometry parameters of the EIRE nanoantenna can effectively affect the properties. For the vertical slots that are isolated from the horizontal slot pair, the resonance frequency f_0 varies linearly as L_1 increases from 190 to 240 nm. The relationship between them is fitted as $f_0 = -0.79L_1 + 372.1$, as shown in Fig. 5(a), while the width of the resonance peak does not change significantly. For the EIRE nanoantenna with the horizontal slot pair, $f_{\rm dip}$ varies linearly as L_2 increases from 400 to 580 nm, and the relationship between them is fitted as $f_{\rm dip} = -0.31L_2 + 341.1$, as shown in Fig. 5(b). When the distance d between the two horizontal slots increases from 120 to 600 nm, the width of the dip broadens slightly due to the increase of the loss of the magnetic octupole antenna, as shown in Fig. 5(c). Figure 5(d) shows the radiation spectra of the antenna with different ITO layer thicknesses. It is seen that for the thin ITO layer ($t_{\rm ITO} < 500$ nm) cases, the increase of $t_{\rm ITO}$ obviously influences the position of the dip in the radiation spectrum. When $t_{\rm ITO} > 500$ nm, the influence is weak and the radiation spectrum remains nearly unchanged.

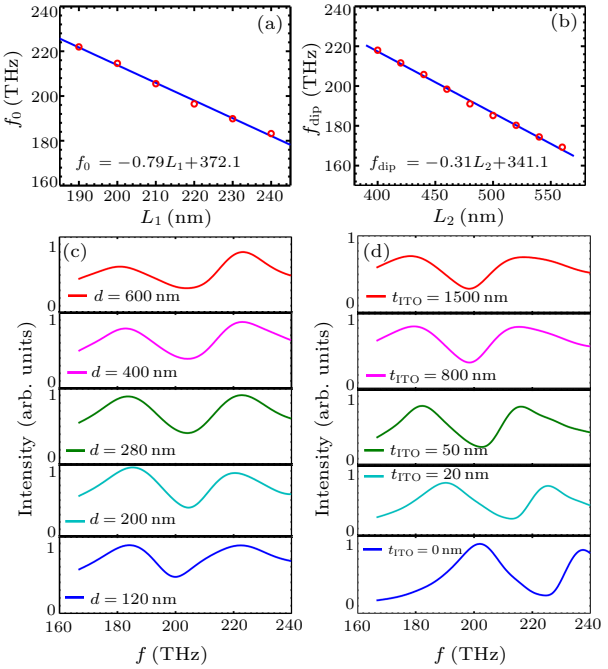

Fig. 5. (a) Variation of f_0 versus L_1 (red circles) and the linear fitting of the results (blue line) for the vertical slots that are isolated from the horizontal slot pair. (b) Variation of $f_{\rm dip}$ of the EIRE nanoantenna versus L_2 (red circles) and the linear fitting of the results (blue line). (c) Normalized radiation spectra of the EIRE nanoantennas with different values of d. (d) Normalized radiation spectra of the EIRE nanoantennas with a different ITO layer thickness $t_{\rm ITO}$.

To provide a quantitative description of our plasmonic EIRE system, we use a simple two-oscillator EIT model.[5,7] The magnetic dipole antennas in our structure are represented by oscillator 1, which is driven by a source $E(t)$. The magnetic octupole antenna is represented by oscillator 2, which can be excited only through coupling between the two oscillators. The charges $q_1(t)$ and $q_2(t)$ in oscillators 1 and 2 satisfy the coupled differential equations

$$\frac{d^2q_1(t)}{dt^2} + \gamma_1\frac{dq_1(t)}{dt} + f_0^2 q_1(t) + \kappa\frac{dq_2(t)}{dt} = E(t), \quad (1)$$

$$\frac{d^2q_2(t)}{dt^2} + \gamma_2\frac{dq_2(t)}{dt} + (f_0+\delta)^2 q_2(t) - \kappa\frac{dq_1(t)}{dt} = 0, \quad (2)$$

where f_0 is the resonance frequency of oscillator 1 when it is isolated from oscillator 2, δ denotes the detuning of the resonance frequency of oscillator 2 from oscillator 1 ($\delta \ll \gamma_1$), which is approximately 2 THz, γ_1 and γ_2 are the dissipation rates in oscillators 1 and 2, respectively ($\gamma_1, \gamma_2 \ll f_0$), which include three contributions, namely, the non-radiative damping due to the intrinsic metal loss, the radiative damping due to the transformation of surface plasmons into photons, and the scattering at the Au film surface and the boundary of the slots. For bulk gold, the permittivity in the infrared spectral regime is described by the Drude model[31,32] with the plasmon frequency $\omega_{\rm pl} = 2\pi \times 2.175 \times 10^{15}\,{\rm s}^{-1}$ and the damping constant $\omega_{\rm c} = 2\pi \times 6.5 \times 10^{12}\,{\rm s}^{-1}$. Owing to the scattering of the surface and boundary of the thin film, in the calculations we use a damping constant that is slightly larger than the value in bulk gold. Moreover, the radiative damping of the magnetic dipole antenna is significantly larger than the magnetic dipole due to the transformation of plasmons into photons. Therefore, according to Ref. [5] we set γ_1 and γ_2 to be 18 and 12 THz in the calculations, respectively. Here κ is the coefficient of the coupling between the two oscillators, which is related to the positions and the distance between them. After solving Eqs. (1) and (2) with the approximation $f - f_0 \ll f_0$ and therefore $f_0^2 - f^2 \approx -2f_0(f - f_0)$, the radiation intensity as a function of frequency is obtained as follows:

$$I(f) \propto \frac{i}{2}\frac{(f - f_0 - \delta) + i\frac{\gamma_2}{2}}{(f - f_0 + i\frac{\gamma_1}{2})(f - f_0 - \delta + i\frac{\gamma_2}{2}) - \frac{\kappa^2}{4}}. \quad (3)$$

Subsequently, we present the results by black curves in Figs. 3(a)–3(d) for a direct comparison with the simulation results. It is evident that the simulation results agree well with the two-oscillator EIT model.

The coupling strength between the magnetic dipole antennas and the magnetic octupole antenna is obviously related to the distance between them. Figure 6(a) shows the relationship between the coupling coefficient κ and g that is calculated by the two-oscillator EIT model. It is seen that κ decreases exponentially as g increases, which is fitted as $\kappa = 53.72e^{-0.021g}$. Another factor that influences the coupling strength is the position of the vertical slots with respect to the horizontal slot pair. When the vertical slots deviate from the middle of the horizontal slot pair, the coupling strength will be weakened, thus the vertical slots should be positioned in the middle of the horizontal slot pair to keep the largest coupling strength.

A large slope in the spectrum is of great significance to improve the sensitivity of refractive index sensors. Various methods have been proposed to achieve a large slope, such as the mode splitting,[33] the EIT-like transmission,[34] the Fano-type resonances,[35,36] and the asymmetric Fano-like line shape based on parity-time symmetry.[37] In this work, the EIRE nanoantenna may serve as an ultracompact sensor in the near infrared since the dip $f_{\rm dip}$ is sensitive to the change of the refractive index n of the medium that is filled in the slots and in the two sides of the Au film. A figure of merit (FOM) defined as FOM=$\Delta I/(I\Delta n)$ is introduced to quantify the performance, where I and ΔI denote the relative radiation intensity of the antenna and the change of I induced by a refractive index change Δn of the medium in the slots. The results with respect to the frequency are calculated, as shown in Fig. 6(b). It is seen that the maximum value reaches as large as 7.61 at $f = 194.5$ THz. The normalized radiation spectra of the EIRE nanoantennas with different n are illustrated in Fig. 6(c). It is seen that at the frequency $f = 194.5$ THz, as n reduces from 1.96 to 1.90, the radiation intensity accordingly reduces from 0.66 to 0.50 with a difference of 0.16. Thus from the variation of the radiation intensity, the changing of the refractive index n can be inferred. Alternatively, the value of n can be sensed from the position of the dip in the radiative spectrum since $f_{\rm dip}$ varies linearly with respect to n, as shown in Fig. 6(d). The relationship between them is fitted as $n = 0.00995 f_{\rm dip} + 3.94$.

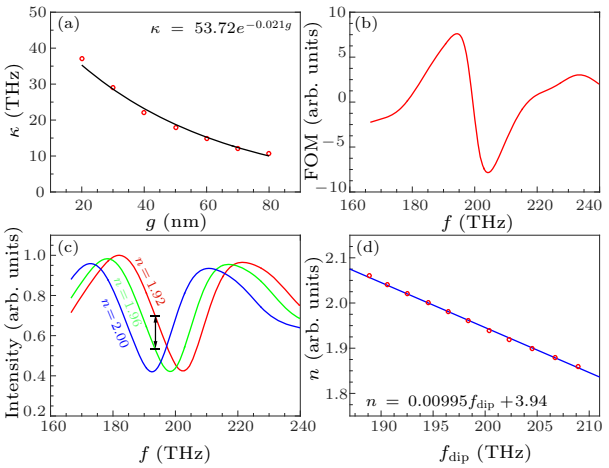

Fig. 6. (a) Variation of the coupling coefficient κ versus g. The red circles represent the simulation results and the black curve is a fitting of them. (b) Variation of FOM versus frequency f. (c) Radiation spectra of the EIRE nanoantenna with different refractive indexes of the medium filled in the slots and in the two sides of the Au film. (d) Relationship between n and $f_{\rm dip}$ and the linear fitting of it.

In conclusion, we have demonstrated a Babinet-inverted optical nanoantenna analogue of electromagnetically induced transparency. A dip has been observed in the radiation spectrum due to the destructive interference between two excitation pathways: the direct excitation of the magnetic dipole antennas by the incident SPs and the excitation by coupling with the magnetic octupole antenna. A two-oscillator EIT model has been used to describe the antenna, which agrees well with the results simulated by the FDTD method. Coupling coefficient between the magnetic dipole antennas and the magnetic octupole antenna

has been calculated, which varies exponentially with respect to the distance between them. Such an antenna has a compact structure and is easy to be fabricated and integrated with optical waveguides, which is of great potential applications in nano-optics.

References

[1] Fleischhauer M, Imamoglu A and Marangos J P 2005 *Rev. Mod. Phys.* **77** 633
[2] Boller J K, Imamoğlu A and Harris S E 1991 *Phys. Rev. Lett.* **66** 2593
[3] Wu Y and Yang X 2005 *Phys. Rev.* A **71** 053806
[4] Lal S, Link S and Halas N J 2007 *Nat. Photon.* **1** 641
[5] Liu N, Langguth L, Weiss T, Kästel J, Fleischhauer M, Pfau T and Giessen H 2009 *Nat. Mater.* **8** 758
[6] Liu N, Weiss T, Mesch M, Langguth L, Eigenthaler U, Hirscher M, Sönnichsen C and Giessen H 2010 *Nano Lett.* **10** 1103
[7] Zhang S, Genov D A, Wang Y, Liu M and Zhang X 2008 *Phys. Rev. Lett.* **101** 047401
[8] Verellen N, Sonnefraud Y, Sobhani H, Hao F, Moshchalkov V V, Dorpe P V, Nordlander P and Maier S A 2009 *Nano Lett.* **9** 1663
[9] Zhu Y, Hu X, Fu Y, Yang H and Gong Q 2013 *Sci. Rep.* **3** 2338
[10] Dong C, Li B, Li H X, Liu H, Chen M Q, Li D D, Yan C C and Zhang D H 2016 *Chin. Phys. Lett.* **33** 074201
[11] Habteyes T G, Dhuey S, Cabrini S, Schuck P J and Leone S R 2011 *Nano Lett.* **11** 1819
[12] Kosako T, Kadoya Y and Hofmann H F 2010 *Nat. Photon.* **4** 312
[13] Novotny L and Hulst N V 2011 *Nat. Photon.* **5** 83
[14] Biagioni P, Huang J S and Hecht B 2012 *Rep. Prog. Phys.* **75** 024402
[15] Olmon R L and Raschke M B 2012 *Nanotechnology* **23** 444001
[16] Garcia-Vidal F J, Martin-Moreno L, Ebbesen T W and Kuipers L 2010 *Rev. Mod. Phys.* **82** 729
[17] Dorfmuller J, Dregely D, Esslinger M, Khunsin W, Vogelgesang R, Kern K and Giessen H 2011 *Nano Lett.* **11** 2819
[18] Dregely D, Taubert R, Dorfmuller J, Vogelgesang R, Kern K and Giessen H 2011 *Nat. Commun.* **2** 267
[19] Taminiau T H, Moerland R J, Segerink F B, Kuipers L and van Hulst N F 2007 *Nano Lett.* **7** 28
[20] Kinkhabwala A A, Yu Z, Fan S, Avlasevich Y, Mullen K and Moerner W E 2009 *Nat. Photon.* **3** 654
[21] Farahani J N, Pohl D W, Eisler J H and Hecht B 2005 *Phys. Rev. Lett.* **95** 017402
[22] Kühn S, Håkanson U, Rogobete L and Sandoghdar V 2006 *Phys. Rev. Lett.* **97** 017402
[23] Muskens O L, Giannini V, Sánchez-Gil J A and Rivas J G 2007 *Nano Lett.* **7** 2871
[24] Curto A G, Volpe G, Taminiau T H, Kreuzer M P, Quidant R and van Hulst N F 2010 *Science* **329** 930
[25] Akimov A V, Mukherjee A, Yu C L, Chang D E, Zibrov A S, Hemmer P R, Park H and Lukin M D 2007 *Nature* **450** 402
[26] Ringler M, Schwemer A, Wunderlich M, Nichtl A, Kürzinger K, Klar T A and Feldmann J 2008 *Phys. Rev. Lett.* **100** 203002
[27] Yang J, Xiao X, Hu C, Zhang W, Zhou S and Zhang J 2014 *Nano Lett.* **14** 704
[28] Zhang J, Zhang W, Zhu X, Yang J, Xu J and Yu D 2012 *Appl. Phys. Lett.* **100** 241115
[29] Kim J, Roh Y G, Cheon S, Choe J H, Lee J, Lee J, Jeong H, Kim U J, Park Y, Song I Y, Park Q H, Hwang S W, Kim K and Lee C W 2014 *Nano Lett.* **14** 3072
[30] Kim J, Roh Y G, Cheon S, Kim U J, Hwang S W, Park Y and Lee C W 2015 *Sci. Rep.* **5** 11832
[31] Johnson P B and Christy R W 1972 *Phys. Rev.* B **6** 4370
[32] Ordal M A, Long L L, Bell R J, Bell S E, Bell R R, Alexander R W and Ward C A 1983 *Appl. Opt.* **22** 1099
[33] Li Q, Wang T, Su Y, Yan M and Qiu M 2010 *Opt. Express* **18** 8367
[34] Xu Q, Sandhu S, Povinelli M L, Shakya J, Fan S and Lipson M 2006 *Phys. Rev. Lett.* **96** 123901
[35] Xiao Y F, Li M, Liu Y C, Li Y, Sun X and Gong Q 2010 *Phys. Rev.* A **82** 065804
[36] Xiao Y F, Gaddam V and Yang L 2008 *Opt. Express* **16** 12538
[37] Li J, Yu R, Ding C and Wu Y 2016 *Phys. Rev.* A **93** 023814